ORIGINAL ARTICLE

Design of optimized halide vapor phase epitaxy (HVPE) conditions for uniform α-Ga$_2$O$_3$ growth based on CFD analysis

Woongchan Kim[1,2] · **Hyeon Woo Kim**[2] · **Sung Beom Cho**[1,2]

Abstract

α-Ga$_2$O$_3$, a metastable ultra-wide bandgap semiconductor, has attracted notable attention for high-power electronics and deep-ultraviolet applications due to its large bandgap and compatibility with sapphire substrates. Halide vapor phase epitaxy (HVPE) is a promising method for the scalable growth of α-Ga$_2$O$_3$, but ensuring high uniformity remains an important challenge, especially as wafer size increases to meet the demands of mass production. Herein, we employed computational fluid dynamics (CFD) and finite element method (FEM) to optimize the heteroepitaxial growth conditions of α-Ga$_2$O$_3$ with the goal of attaining high deposition uniformity. First, we conducted a parametric study to evaluate how four critical parameters—carrier gas flow rate, outer gas flow rate, growth temperature, and susceptor distance—affect uniformity. Gaussian process regression was then applied to identify the optimal set of process parameters for enhanced uniformity. The resulting simulation findings provide a theoretical framework for optimizing HVPE growth conditions for α-Ga$_2$O$_3$, facilitating the way for highly uniform deposition on increasingly larger substrates.

Keywords α-Ga$_2$O$_3$ · HVPE · Uniformity · CFD · Optimization

1 Introduction

The development of thin-film growth techniques plays a crucial role in advancing material synthesis and enabling the fabrication of novel and more efficient semiconductor devices [1–7]. Various deposition methods, such as molecular beam epitaxy (MBE) [8], metal–organic chemical vapor deposition (MOCVD) [9], and chemical vapor deposition (CVD), have been widely investigated to optimize thin-film quality, growth rate, and scalability. Among these techniques, halide vapor phase epitaxy (HVPE) [10] has emerged as a widely used method due to its high deposition rate, cost-effectiveness, and ability to grow high-quality films with relatively low impurity concentrations. HVPE is particularly advantageous for the fabrication of compound semiconductor materials, as it utilizes halogen-based precursors to transport metal species in the vapor phase, enabling

efficient and controlled epitaxial growth. The process typically involves reacting hydrogen chloride (HCl) with a metallic source to generate volatile metal halides, which are subsequently transported to the growth zone, where they react with oxidizing or nitridizing agents to form the desired thin film. Compared to other vapor-phase growth techniques, HVPE offers significant benefits in terms of throughput and material purity, making it a promising candidate for large-scale semiconductor manufacturing [11, 12].

Despite its advantages, ensuring high uniformity across large substrates remains a key challenge in HVPE processing. As wafer sizes continue to increase to meet industrial-scale demands, issues related to non-uniform precursor transport, thermal gradients, and parasitic gas-phase reactions become more pronounced. Such challenges are important for Ga$_2$O$_3$ materials, where achieving high crystalline quality and uniformity is essential for growth and device applications [13, 14]. In particular, α-Ga$_2$O$_3$ epitaxy is highly sensitive to gas-phase pre-reactions, which can cause homogeneous nucleation and result in the formation of unwanted particles [15–21]. Such particles may incorporate into the growing film or deposit on reactor walls, thereby increasing surface roughness and defect density, and ultimately degrading epitaxy quality. Hence, precise control

✉ Sung Beom Cho
  csb@ajou.ac.kr

1 Department of Energy Systems Research, Ajou University, Suwon, Gyeonggi-do 16499, Republic of Korea

2 Department of Material Science and Engineering, Ajou University, Suwon, Gyeonggi-do 16499, Republic of Korea

overgrowth conditions is critical to produce high-quality, uniform α-Ga$_2$O$_3$ films. To address these challenges, computational fluid dynamics (CFD) simulations have been widely employed to analyze and optimize HVPE reactor conditions [22]. CFD modeling provides insights into gas flow dynamics, thermal distributions, and mass transport mechanisms, enabling the refinement of key process parameters, such as gas flow rate and growth temperature. By optimizing these factors, researchers aim to achieve more uniform deposition and suppress undesirable effects—including precursor depletion, homogeneous nucleation, and defect formation—thereby improving the overall quality of α-Ga$_2$O$_3$ epitaxy.

In this study, we employed computational fluid dynamics (CFD) simulations and finite element method (FEM) analyses to investigate the factors influencing uniformity and to optimize process parameters in an HVPE reactor designed for α-Ga$_2$O$_3$ growth. To systematically examine the relationship between individual process variables and film uniformity, we performed a parametric study by varying one parameter at a time while keeping all others constant. By precisely adjusting carrier and outer gas flow rates, growth temperature, and susceptor position, we identified optimized combination to improve epitaxy uniformity. Subsequently, we applied a stratified Monte Carlo sampling approach to generate 125 data points, utilizing Gaussian process regression to establish a process window that mitigates homogeneous nucleation. This approach allowed us to refine HVPE conditions for stable, uniform film growth at larger scales. The findings provide a framework for optimizing α-Ga$_2$O$_3$ deposition and reactor design, contributing to its scalable production for power electronics and optoelectronic applications.

2 Methods

The finite element method (FEM) was employed to model the HVPE process using COMSOL Multiphysics. Two governing physics were considered: fluid dynamics and heat transfer. To simulate gas flow within the chamber, the turbulent flow equations were applied, ensuring an accurate representation of flow behavior. Heat transfer was modeled through conduction and convection, accounting for the effects of the heater near the source and growth zones, as well as heat exchange via the gas flow (precursor, carrier gas, and outer gas).

The turbulent flow model was used to analyze the velocity and pressure fields in a single-phase gas environment, capturing complex flow patterns generated by multiple injection points. Carrier and outer gases were injected to simulate realistic operating conditions and examine flow variations. A framework incorporating the Navier–Stokes equations with

appropriate turbulence modeling was adopted to accurately represent vortex formation and flow instabilities:

$$\rho(u \cdot \nabla)u = \nabla \cdot \left[-pI + \left(\mu + \mu_T \right)\left(\nabla u + \left(\nabla u \right)^T \right) \right] + F$$

$$\rho \nabla \cdot u = 0$$

Here, ρ represents the fluid density, u denotes the velocity field, p is the pressure, μ is the viscosity, μ_T corresponds to the turbulent viscosity, T indicates the transpose, and F represents external forces acting on the fluid. The equations are solved under stationary boundary conditions, with dense sampling of the background gas flow, outer gas flow, growth temperature, and variations in the susceptor position.

Heat transfer model was used to analyze the temperature distribution in chamber by gas flow. Considering the convection and conduction, temperature distribution was calculated by following equations:

$$\rho C_{\mathrm{p}} u \cdot \nabla T + \nabla \cdot q = Q$$

$$q = -k \nabla T$$

where C_{p} is the heat capacity at constant pressure, T is temperature, q is heat flux, Q is heat source, and k is thermal conductivity.

In the simulation setup, both the initial chamber pressure and the outlet pressure were fixed at 1 atm (760 Torr) to replicate a typical atmospheric-pressure HVPE process. This configuration reflects a condition in which gases are introduced through the inlets at fixed flow rates and exit the reactor under ambient pressure. In addition, the inlet gas temperature was set to room temperature (298.15 K), consistent with the experimental configuration [20]. Gas properties and thermal conductivity were treated as temperature- and pressure-dependent, based on the material database provided by COMSOL Multiphysics. Boundary conditions were assigned as follows: the HCl inlet flow rate was fixed at 15 sccm, and the outlet was treated as a pressure outlet at 1 atm (760 Torr). For the reaction and growth zones, fixed temperature values were used as boundary conditions.

3 Results

Figure 1 provides a schematic overview of HVPE process for α-Ga$_2$O$_3$, highlighting the key variables, including carrier gas flow, outer shell gas flow, susceptor distance, and growth temperature. The process typically unfolds in two main zones: a source zone and a growth zone. In the source zone, HCl gas—delivered by a carrier gas (N$_2$)—reacts with liquid gallium to form gallium chlorides (GaCl or GaCl$_3$). These gaseous intermediates then flow into the growth zone,

Fig. 1 Geometric diagram of the Ga$_2$O$_3$ HVPE model, including the working conditions, such as carrier gas flow rate, outer gas flow rate, growth temperature, and susceptor position
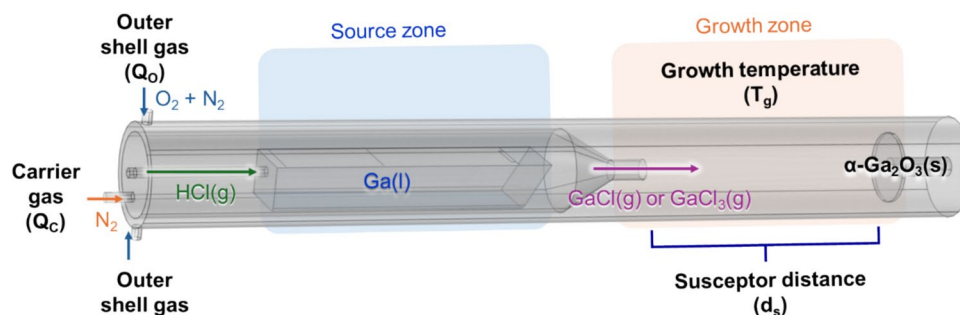

Table 1 Key process parameters used for the optimization of α-Ga$_2$O$_3$ HVPE growth

Carrier gas flow rate (Q_C, sccm)	Outer gas flow rate (Q_O, sccm)	Growth temperature (T_g, °C)	Susceptor distance (d_s, cm)
1000	**200**	420	5
2000	600	445	7
3000	1000	**470**	9
4000	1400	495	**11**
5000	1800	520	13

Default values used in simulations are indicated in bold

where they encounter an outer gas mixture of O$_2$ and N$_2$ on a heated sapphire substrate mounted on a susceptor. Specifically, the reaction between GaCl or GaCl$_3$ and O$_2$ gas should occur on the substrate to avoid detrimental pre-reactions that degrade film quality. Therefore, under carefully controlled temperatures, gas flow, and reactor design, the HVPE process can be fine-tuned to meet the strict requirements for uniform and high-quality thin films.

Among the many factors that can influence the uniformity of α-Ga$_2$O$_3$ thin films, this study focused on four key parameters: carrier gas flow rate, outer gas flow rate, growth zone temperature, and susceptor distance. Because the HCl gas flow rate is fixed at 15 sccm, which is relatively low to

maintain the stoichiometry required for Ga$_2$O$_3$ formation, the carrier gas flow rate predominantly governs overall gas flow behavior. We further hypothesized that variations in the outer gas flow rate can alter gas dynamics within the growth zone, thereby affecting film uniformity. Growth zone temperature also plays a crucial role, as thermal gradients near the substrate can notably modify local gas flow patterns and deposition processes. Finally, the susceptor distance, defined as the distance from the source zone outlet to the susceptor surface in the growth zone, can influence the local growth environment and ultimately affect film uniformity. By optimizing these four parameters, we aimed to improve α-Ga$_2$O$_3$ uniformity and clarify each parameter's individual impact on the HVPE growth process.

After identifying the default parameters and their ranges (summarized in Table 1), we carried out CFD simulations for the HVPE of α-Ga$_2$O$_3$. Our primary goals were to examine how gas flow behavior and heat transfer influence processes inside the chamber. As shown in Fig. 2a, the carrier gas enters the reactor, flows over the Ga-containing boat, and proceeds toward the growth zone. Owing to the reactor's geometry, a recirculating flow forms near the outlet, potentially affecting gas residence time and the mixing of species. This can influence the uniformity of precursor delivery to the substrate. Figure 2b, c reveals that velocity and temperature vary throughout the reactor. For instance,
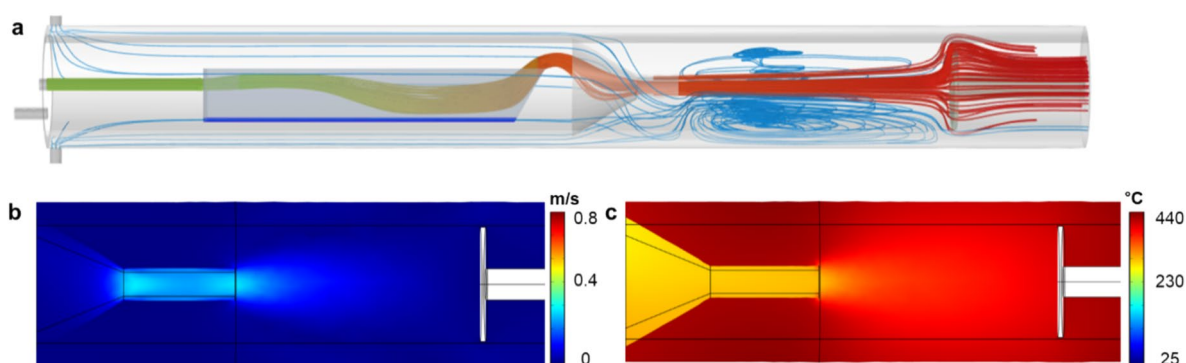

Fig. 2 Computational fluid dynamics (CFD) simulation results for the HVPE process of α-Ga$_2$O$_3$. **a** Streamline visualization. **b** Velocity distribution (m/s) in the horizontal plane. **c** Temperature distribution (°C) in the horizontal plane

while the gas enters with a velocity of around 0.27 m/s in the supply region, it slows considerably near the susceptor—down to roughly 0.0016 m/s. Such a substantial drop in velocity around the substrate can have implications for growth rate uniformity across the wafer. In addition, when the gases move from a wider inlet to the narrower chamber section, they experience a constriction that raises their velocity. In this transition, the interaction of the carrier gas with surrounding flows can create localized eddies, further contributing to non-uniform transport of gas-phase species.

In terms of thermal distribution, the growth zone exhibits a lower temperature than the intended growth temperature of 470 °C, with the substrate experiencing an actual chamber temperature of around 404 °C. This discrepancy arises due to the rapid influx of cooler gas, which induces localized cooling effects and highlights the impact of forced convective heat transfer on the overall thermal profile within the reactor. Given that a uniform temperature distribution is essential for maintaining consistent growth conditions, these findings underscore the importance of carefully tuning process parameters, such as gas flow rate and reactor geometry. By understanding how these factors influence velocity fields and thermal gradients, process conditions can be optimized to enhance uniformity and reproducibility in α-Ga$_2$O$_3$ heteroepitaxy, ultimately leading to better control over material quality and device performance.

Building on these insights, we now present the results of our parametric study, which examines the effects of key processing parameters—carrier gas flow rate, outer gas flow rate, growth temperature, and susceptor distance—on the reactor environment. As summarized in Table 1, we systematically varied each parameter while keeping the others at their default values, and the results are organized in Figs. 3 and S1–S3. Figure 3 specifically highlights the impact of carrier gas flow rate on the velocity field and temperature distribution within the reactor. The carrier gas flow rate plays a dominant role in determining the overall gas dynamics, affecting both velocity and thermal profiles. As the flow rate increases from 1000 to 5000 sccm, the maximum velocity near the substrate rises from 0.25 to 5.0 cm/s, which is expected, because the carrier gas predominantly dictates the flow behavior within the chamber. The enhanced gas flow also influences the thermal environment, causing a noticeable cooling effect: the maximum substrate temperature decreases from approximately 404 to 329 °C, exhibiting an inverse relationship with flow rate. This cooling effect arises from the increased influx of lower-temperature gas, which enhances convective heat removal from the substrate surface.

Continuing our parametric study, we also investigated how variations in outer gas flow rate, growth zone temperature, and susceptor position affect flow and thermal distributions. Figure 4a illustrates the impact of the outer gas flow rate on the velocity field and temperature distribution. Compared to the carrier gas flow, the outer gas flow rate applies only a minor effect on velocity near the substrate. Even as the flow rate increases from 200 to 1800 sccm, the
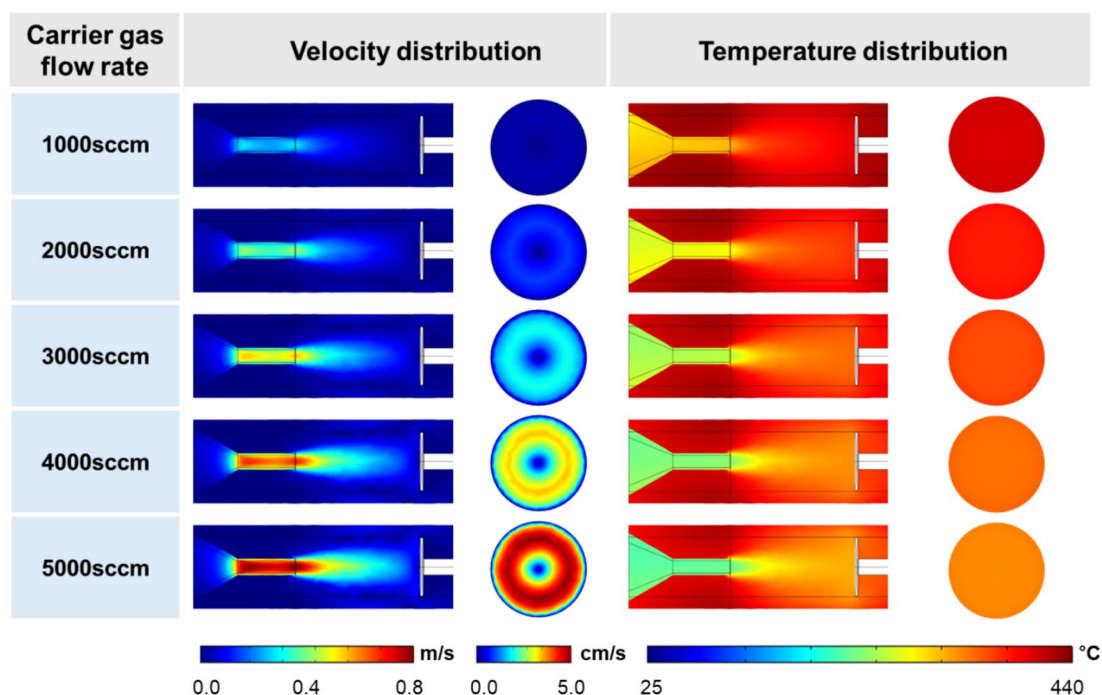

Fig. 3 Parametric study results on the effect of carrier gas flow rate. From left to right: velocity field cross section of the growth zone, velocity field on surface of the susceptor, temperature cross section of the growth zone, and surface temperature distribution of the susceptor
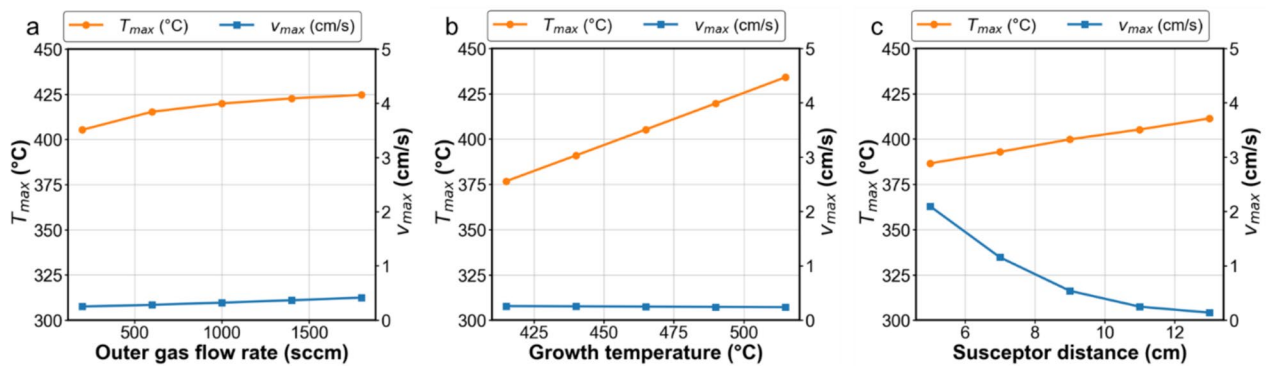
Fig. 4 Maximum temperature and velocity on the substrate under different process conditions: **a** outer gas flow rate, **b** growth temperature, and **c** susceptor distance

maximum velocity in the growth zone rises only slightly—from 0.25 to 0.41 cm/s—highlighting its limited effect. This is largely due to reactor geometry: while the carrier gas flows through a confined region and directly drives the main velocity field, the outer gas disperses into a larger volume before reaching the growth zone, diluting its impact on localized flow dynamics. In contrast, the temperature shows a noticeable increase with higher outer gas flow rates. Because the outer gas region is located near the heat source—defined as the chamber wall, which is subject to a fixed high-temperature boundary condition—and subject to turbulent mixing, greater flow enhances heat exchange. This leads to an increase in the maximum temperature from roughly 404 to 424 °C.

Figure 4b, meanwhile, shows the effect of growth zone temperature on flow behavior. As the growth temperature is raised, the maximum velocity near the substrate remains nearly unchanged (0.26 to 0.24 cm/s), indicating that the overall flow field is predominantly driven by forced convection from the incoming gas stream. Despite the cooling influence of the cold gas flow, the maximum temperature still rises along with the set growth temperature. Finally, Fig. 4c depicts how changing the susceptor's position alters both flow and temperature. When the susceptor is positioned closer to the carrier gas inlet, the substrate experiences higher velocity and lower temperature, due to direct exposure to the incoming flow. However, increasing the susceptor distance from 5 to 13 cm reduces the velocity near the substrate from 2.11 to 0.10 cm/s while allowing the temperature to rise from 386 to 411 °C. These findings underscore how reactor geometry, in addition to gas flow parameters and growth temperature, can critically shape the local growth environment. For further details, Figures S1, S2 and S3 illustrate the combined effects of these parameters on flow and thermal behavior.

Building on these insights into how process parameters affect both the velocity field and temperature, we now turn

to their impact on uniformity under steady-state conditions. To quantify non-uniformity, we define w_T and w_v as the differences between the maximum and minimum temperature and velocity on the substrate surface, respectively. Figure 5 presents these non-uniformity metrics for various parameter settings. In Fig. 5a, the carrier gas flow rate emerges as the dominant factor determining w_v. As the carrier gas flow rate increases, the velocity difference across the growth zone decreases, improving asymmetry. This occurs, because the high-momentum inflow from the source zone suppresses localized variations while making flow asymmetric. A similar trend is observed for w_T at high flow rates, where momentum concentration near the inlet is significant, though no clear correlation appears at lower flow rate.

Figure 5b examines the effect of the outer gas flow rate. Because outer flow exerts a smaller influence on the overall velocity distribution, w_v shows only a weak dependence on changes in outer gas flow. However, w_T decreases with increasing outer gas flow rate, indicating improved thermal uniformity. This can be attributed to enhanced mixing between the hotter outer gas and the carrier gas, which helps even out the overall temperature field. Figure 5c explores the influence of the growth temperature. The w_v trend remains largely unchanged, in line with the findings from Figure S2, which highlight that growth temperature minimally affects the gas flow itself. However, temperature non-uniformity increases likely due to the temperature gradient between the hotter substrate edges (strongly influenced by the heat source) and the substrate center (more directly exposed to the cooler incoming carrier gas). Finally, Fig. 5d reveals how the susceptor distance affects velocity and temperature distributions. Both w_v and w_T decrease as the susceptor is moved farther from the source zone, because the cool carrier gas must travel farther to reach the substrate, reducing its localized cooling effect. As a result, heat from the source becomes more dominant, lowering overall gradients in both velocity and temperature.
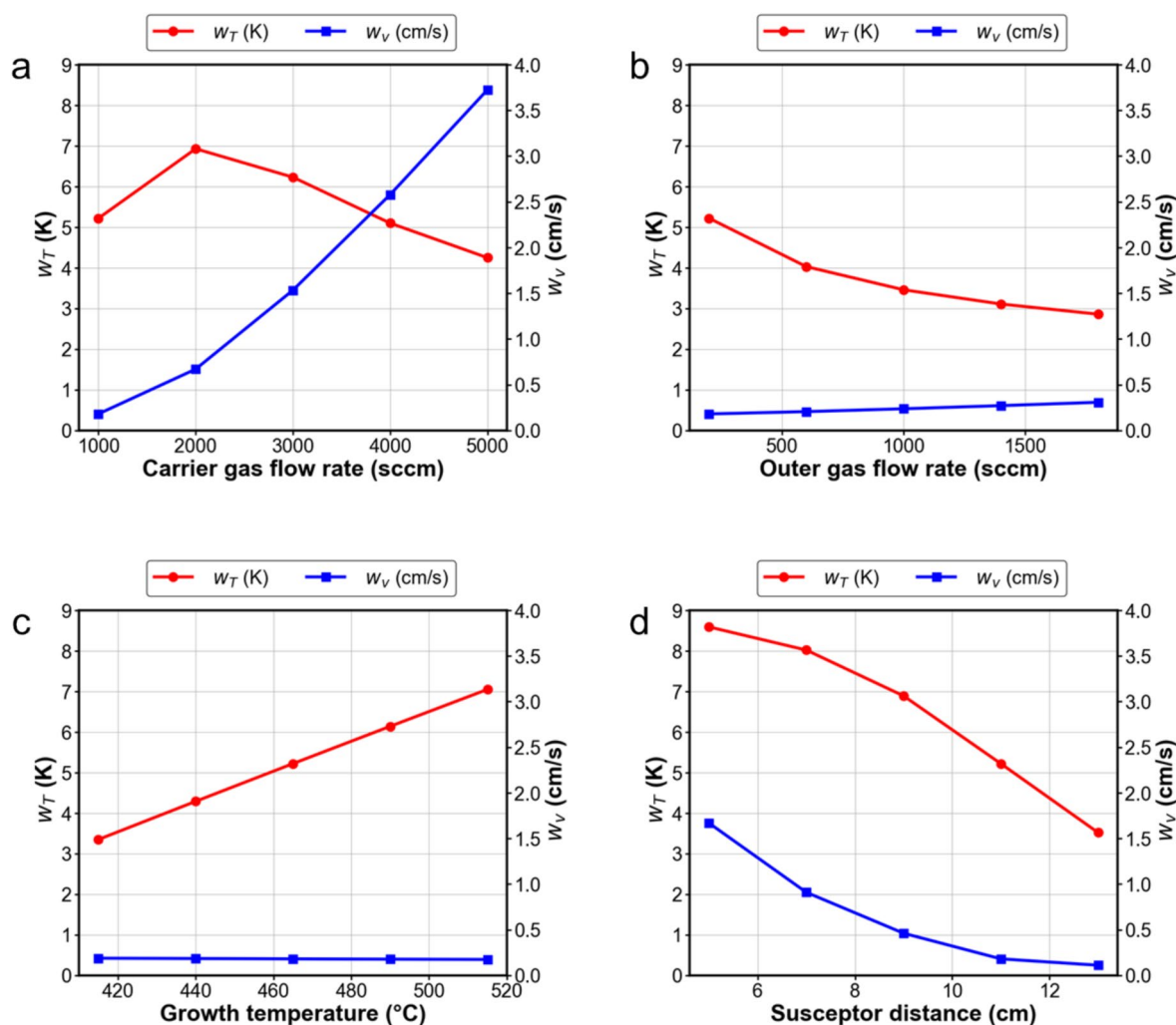
Fig. 5 Variation of temperature non-uniformity (w_T) and velocity non-uniformity (w_v) on the substrate under different process conditions: **a** carrier gas flow rate, **b** outer gas flow rate, **c** growth temperature, and **d** susceptor distance

Based on our parametric study, we established a relationship between key process parameters and uniformity. We then leveraged this information to optimize the parameters for higher uniformity. To achieve this, we employed stratified Monte Carlo sampling, which ensures systematic exploration of the parameter space by evenly distributing samples across predefined ranges. [23] In total, we generated 125 samples to ensure uniform coverage across the parameter ranges, facilitating an extensive analysis of the influence of these parameters on uniformity. After selecting the samples, we used Gaussian Process Regression (GPR) to model the relationship between the process parameters and uniformity [24]. GPR provides predictive distributions with uncertainty estimates, accommodates complex parameter interactions via kernel functions, and maintains reliable performance even with relatively small data sets. In our approach, the process parameters served as input features, while w_v and w_T were used as target labels for velocity and temperature

non-uniformity, respectively. The results of this training are summarized in Table 2. Notably, high R^2 values (0.959 for w_v and 0.998 for w_T) and correspondingly low RMSE values (1.36×10^{-7} for w_v and 5.28×10^{-3} for w_T) emphasize the accuracy of the predictive model and confirm that GPR effectively captures the underlying relationships between the parameters and the uniformity indices.

In our optimization process, we set the growth temperature to 470 °C because of its pivotal influence on absorption,

Table 2 Summary of Gaussian process regression (GPR) model performance for predicting velocity (w_v) and temperature (w_T) non-uniformity

Target variable	R^2 value	RMSE
w_v	0.959	1.36×10^{-7} cm/s
w_T	0.998	5.28×10^{-3} K

nucleation, and overall film deposition. We then focused primarily on optimizing the carrier gas flow rate, external gas flow rate, and susceptor distance. In addition, we incorporated a penalty function following a previously reported strategy, which demonstrated that insufficient asymmetric flow can lead to a high driving force for homogeneous nucleation of Ga_2O_3 in the gas phase—ultimately degrading uniformity and film quality. To reflect these conditions, we applied a linear penalty function whenever the maximum velocity on the substrate was below 0.025 cm/s, thus assigning proportionally greater penalties to lower flow velocities.

Figure 6 shows normalized uniformity (ranging from 0 to 1, where higher values indicate better uniformity) as a function of carrier gas flow rate (Qc) and outer gas flow rate (Qo) for five different susceptor distances (5 cm, 7 cm, 9 cm, 11 cm, and 13 cm). Each panel highlights how shifting the

susceptor alters the balance between these two flow rates, with the optimal points (stars) marking the highest uniformity for each distance. A closer inspection reveals several important trends. At shorter susceptor distances (5 and 7 cm), high uniformity regions tend to occur at moderate Qc combined with relatively high Qo, suggesting that the outer gas flow helps stabilize temperature and flow profiles at close spacing. However, as the susceptor distance increases (9 to 13 cm), the optimal solution shifts toward larger Qc values, indicating that carrier gas flow becomes more critical for maintaining an appropriate velocity field and preventing excessive homogeneous nucleation. This shift is consistent with the reactor geometry: when the susceptor is farther from the inlet, a stronger carrier gas flow compensates for the longer flow path and ensures sufficient asymmetry to avoid stagnation or overly symmetric gas flow patterns.
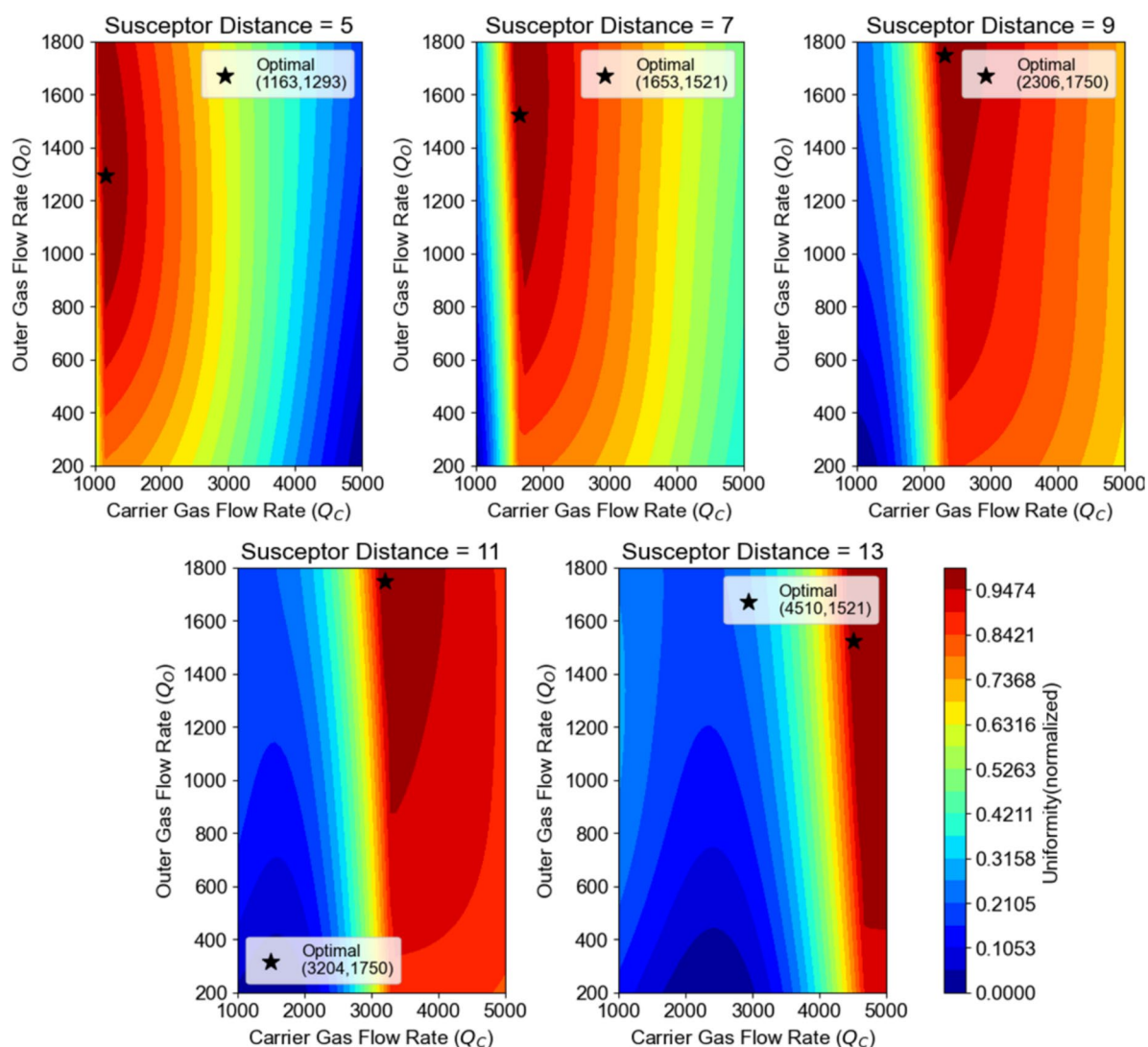

Fig. 6 Contour plots of the normalized uniformity as a function of carrier gas flow rate (Qc) and outer gas flow rate (Q_O) at different susceptor distances

Moreover, the penalty function encourages adequate flow and mixing by penalizing low-velocity conditions. The contour plots smoothly transition from blue (poor uniformity) to red (excellent uniformity), reflecting incremental improvements and suggesting that small variations near the optimum may still achieve reasonable uniformity. Steeper gradients in certain regions highlight the delicate balance between thermal and flow dynamics.

Finally, we emphasize the importance of uniformity particularly for larger wafer sizes. To assess the impact of wafer size on uniformity, we conducted simulations with a 10% larger substrate and compared the results with our default parameters (baseline) in Fig. 7. In the baseline, w_T was 5.22 K and w_v was 0.181 cm/s. When the wafer size increased by 10%, w_T increased to 6.79 K (30.08% increase) and w_v rose to 0.234 cm/s (29.28% increase). This result highlights that increasing wafer size amplifies non-uniformity in both temperature and velocity fields. The observed rise in w_T suggests that thermal gradients become more pronounced in a larger wafer, potentially leading to variations in material properties across the surface. Similarly, the increase in w_v indicates greater velocity fluctuations, which could impact precursor transport and deposition uniformity. These findings highlight the necessity of further optimization when scaling up wafer dimensions to maintain consistent film quality. Future studies can explore strategies to mitigate non-uniformity in larger wafers, such as adaptive thermal management or optimized flow dynamics, to further enhance scalability and industrial applicability.

4 Conclusion

In summary, we provided a comprehensive optimization strategy for heteroepitaxial growth of α-Ga$_2$O$_3$ via HVPE. Using computational fluid dynamics (CFD) simulations, we examined how four key parameters—carrier gas flow rate, outer gas flow rate, growth temperature, and susceptor distance—affect reactor flow dynamics, substrate temperature distribution, and overall uniformity for epitaxy. Our parametric investigation revealed that the carrier gas flow rate strongly influences flow behavior and temperature, and uniformity. On the other hand, the outer gas flow rate, growth temperature, and susceptor distance do not significantly affect gas flow behavior, but they play a crucial role in ensuring uniform α-Ga$_2$O$_3$ films by governing the thermal environment. Furthermore, Gaussian process regression was employed to propose process conditions that both prevent pre-reactions and ensure optimal film uniformity, emphasizing the importance of precise process control in α-Ga$_2$O$_3$ growth. These findings establish a comprehensive theoretical framework for tailoring HVPE conditions to achieve uniform α-Ga$_2$O$_3$ films. Moreover, our approach can guide the optimization of other semiconductor materials beyond Ga$_2$O$_3$,
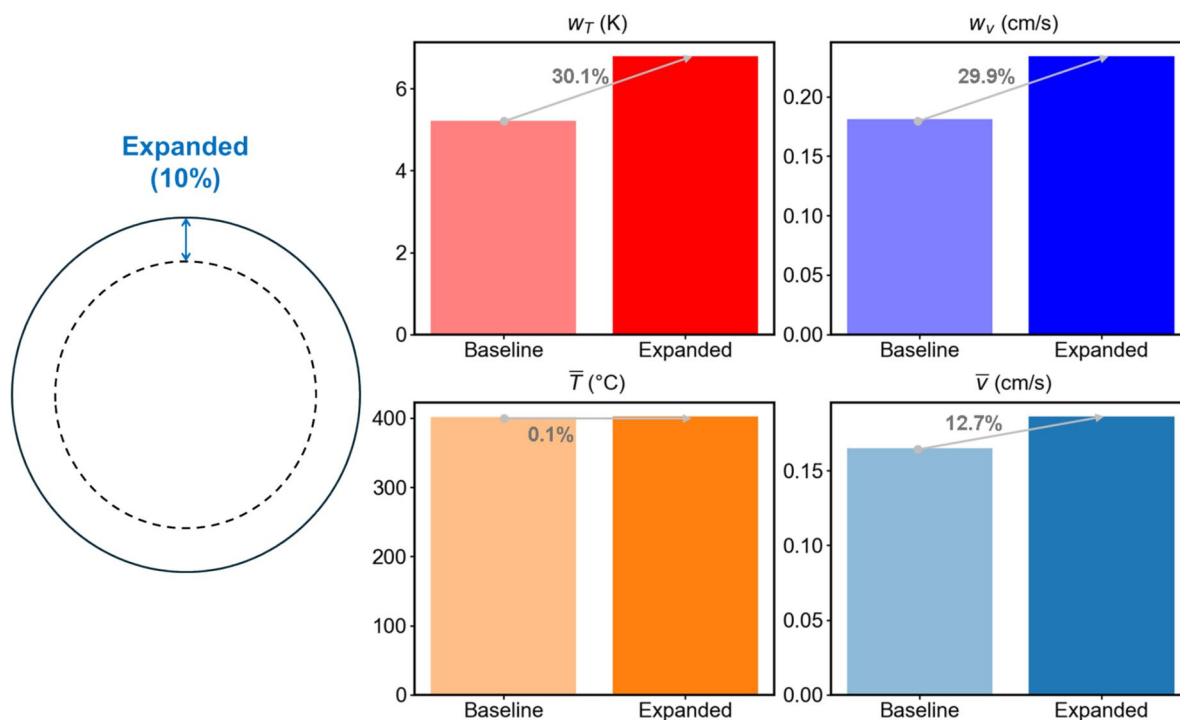

Fig. 7 Comparison of flow characteristics between baseline and expanded (10%) cases for w_T, w_v, average temperature (T), and average velocity ($\bar{v}$)

and it can be broadly applied not only to HVPE processes but also to other CVD processes with similar mechanisms.

Data availability The datasets used and/or analysed during the current study available from the corresponding author on reasonable request.

Declarations

Conflict of interest All authors declare that there are no conflicts of interest in connection with this work.

References

1. A. Ghazanfari, C. Perreault, K. Zaghib, EV/HEV industry trends of wide-bandgap power semiconductor devices for power electronics converters. In 2019 IEEE 28th Int. Symp. Ind. Electron. (ISIE) 2019, vol. 00, pp. 1917–1923. https://doi.org/10.1109/isie.2019.8781528

2. Y.J. Jeong, J.-H. Park, M.J. Yeom, I. Kang, J.Y. Yang, H.-Y. Kim, D.-W. Jeon, G. Yoo, Heteroepitaxial α-Ga_2O_3 MOSFETs with a 2.3 KV breakdown voltage grown by halide vapor-phase epitaxy. Appl. Phys. Express **15**(7), 074001 (2022). https://doi.org/10.35848/1882-0786/ac7431

3. J.-S. Li, H.-H. Wan, C.-C. Chiang, T.J. Yoo, M.-H. Yu, F. Ren, H. Kim, Y.-T. Liao, S.J. Pearton, Breakdown up to 13.5 KV in NiO/β-Ga_2O_3 vertical heterojunction rectifiers. ECS J. Solid State Sci. Technol. **13**(3), 035003 (2024). https://doi.org/10.1149/2162-8777/ad3457

4. J.K. Mun, K. Cho, W. Chang, H.-W. Jung, J. Do, Editors' choice—2.32 KV breakdown voltage lateral β-Ga_2O_3 MOSFETs with source-connected field plate. ECS J. Solid State Sci. Technol. **8**(7), Q3079–Q3082 (2019). https://doi.org/10.1149/2.0151907jss

5. Z. Hu, H. Zhou, Q. Feng, J. Zhang, C. Zhang, K. Dang, Y. Cai, Z. Feng, Y. Gao, X. Kang, Y. Hao, Field-plated lateral β-Ga_2O_3 Schottky barrier diode with high reverse blocking voltage of more than 3 KV and high DC power figure-of-merit of 500 MW/Cm^2. IEEE Electron Device Lett. **39**(10), 1564–1567 (2018). https://doi.org/10.1109/led.2018.2868444

6. A. Matallana, E. Ibarra, I. López, J. Andreu, J.I. Garate, X. Jordà, J. Rebollo, Power module electronics in HEV/EV applications: new trends in wide-bandgap semiconductor technologies and design aspects. Renew. Sustain. Energy Rev. **113**, 109264 (2019). https://doi.org/10.1016/j.rser.2019.109264

7. S.M.S.H. Rafin, R. Ahmed, O.A. Mohammed, Wide band gap semiconductor devices for power electronic converters. In 2023 Fourth Int. Symp. 3D Power Electron. Integr. Manuf. (3D-PEIM) 2023, vol. 00, pp. 1–8. https://doi.org/10.1109/3d-peim55914.2023.10052586

8. T. Oshima, T. Okuno, S. Fujita, Ga_2O_3 thin film growth on C-plane sapphire substrates by molecular beam epitaxy for deep-ultraviolet photodetectors. Jpn. J. Appl. Phys. **46**(11R), 7217 (2007). https://doi.org/10.1143/jjap.46.7217

9. K. Akaiwa, K. Kaneko, K. Ichino, S. Fujita, Conductivity control of Sn-doped α-Ga_2O_3 thin films grown on sapphire substrates. Jpn. J. Appl. Phys. **55**(12), 1202BA (2016). https://doi.org/10.7567/jjap.55.1202ba

10. M. Lee, M. Yang, H.-Y. Lee, H.U. Lee, H. Lee, H. Son, U.J. Kim, The growth of HVPE α-Ga_2O_3 crystals and its solar-blind UV photodetector applications. Mater. Sci. Semicond. Process. **123**, 105565 (2021). https://doi.org/10.1016/j.mssp.2020.105565

11. K. Uno, M. Ohta, I. Tanaka, Growth mechanism of α-Ga_2O_3 on a sapphire substrate by mist chemical vapor deposition using acetylacetonated gallium source solutions. Appl. Phys. Lett. **117**(5), 052106 (2020). https://doi.org/10.1063/5.0014056

12. S.H. Kim, M. Yang, H.-Y. Lee, J.-S. Choi, H.U. Lee, U.J. Kim, M. Lee, Structural characteristics of α-Ga_2O_3 films grown on sapphire by halide vapor phase epitaxy. Mater. Sci. Semicond. Process. **123**, 105534 (2021). https://doi.org/10.1016/j.mssp.2020.105534

13. J. Lee, D. Oh, D. Kwon, Y. Kim, Optimization of β-Ga_2O_3 epitaxial growth via mist CVD by controlling susceptor position. J. Korean Inst. Electr. Electron. Mater. Eng. **36**(5), 500–504 (2023). https://doi.org/10.4313/JKEM.2023.36.5.10

14. S. Lee, J. Jung, Y. Park, Y. Kim, Electrical characteristics of β-Ga_2O_3 vertical Schottky barrier diodes with different guard ring structures. J. Korean Inst. Electr. Electron. Mater. Eng. **37**(2), 208–214 (2024). https://doi.org/10.4313/JKEM.2024.37.2.13

15. K. Kaneko, S. Fujita, T. Shinohe, K. Tanaka, Progress in α-Ga_2O_3 for practical device applications. Jpn. J. Appl. Phys. **62**(SF), SF0803 (2023). https://doi.org/10.35848/1347-4065/acd125

16. Y. Oshima, K. Kawara, T. Oshima, M. Okigawa, T. Shinohe, Rapid growth of -Ga_2O_3 by HCl-boosted halide vapor phase epitaxy and effect of precursor supply conditions on crystal properties. Semicond. Sci. Technol. **35**(5), 055022 (2020). https://doi.org/10.1088/1361-6641/ab7843

17. Z. Wen, K. Khan, K. Sun, R. Wellen, Y. Oshima, E. Ahmadi, Thermal stability of HVPE-grown (0001) α-Ga_2O_3 on sapphire template under vacuum and atmospheric environments. J. Vac. Sci. Technol. A **41**(4), 043403 (2023). https://doi.org/10.1116/6.0002559

18. H. Son, D.-W. Jeon, Optimization of the growth temperature of α-Ga_2O_3 epilayers grown by halide vapor phase epitaxy. J. Alloy. Compd. **773**, 631–635 (2019). https://doi.org/10.1016/j.jallcom.2018.09.230

19. K. Kawara, Y. Oshima, M. Okigawa, T. Shinohe, Elimination of threading dislocations in α-Ga_2O_3 by double-layered epitaxial lateral overgrowth. Appl. Phys. Express **13**(7), 075507 (2020). https://doi.org/10.35848/1882-0786/ab9fc5

20. S. Kim, H.W. Kim, H.-Y. Kim, D.-W. Jeon, S.B. Cho, J.-H. Park, A pre-reaction suppressing strategy for α-Ga_2O_3 halide vapor pressure epitaxy using asymmetric precursor gas flow. CrystEngComm **24**(16), 3049–3056 (2022). https://doi.org/10.1039/d2ce00222a

21. S.A. Safvi, N.R. Perkins, M.N. Horton, R. Matyi, T.F. Kuech, Effect of reactor geometry and growth parameters on the uniformity and material properties of GaN sapphire grown by hydride vapor-phase epitaxy. J. Cryst. Growth **182**(3–4), 233–240 (1997). https://doi.org/10.1016/s0022-0248(97)00375-8

22. Y. Wu, C. Chen, J. Yu, G. Wang, S. Wang, L. Liu, G. Liu, X. Xu, L. Zhang, Optimizing HVPE flow field to achieve GaN crystal

uniform growth. J. Cryst. Growth **614**, 127214 (2023). https://doi.org/10.1016/j.jcrysgro.2023.127214

23. A. Carpentier, R. Munos, A. Antos, Adaptive strategy for stratified Monte Carlo sampling. J. Mach. Learn. Res. **16**, 2231–2271 (2015). https://www.jmlr.org/papers/v16/carpentier15a.html

24. E. Schulz, M. Speekenbrink, A. Krause, A tutorial on Gaussian process regression: modelling, exploring, and exploiting functions. J. Math. Psychol. **85**, 1–16 (2018). https://doi.org/10.1016/j.jmp.2018.03.001